1 **Correlation of Nasal Morphology to Air-Conditioning and Clearance**
2 **Function.**
3

4 David E. White[a], Ahmed M. Al-Jumaily[a], James Bartley[b], Jun Lu[a]

5

6 [a] Institute of Biomedical Technologies, Auckland University of Technology, Auckland, New

7 Zealand.

8 [b] Department of Surgery, University of Auckland, Auckland, New Zealand.

9

10

11 **Corresponding Author:**

12 Professor Ahmed M. Al-Jumaily

13 Institute of Biomedical Technologies,

14 Auckland University of Technology,

15 Private Bag 92006,

16 Auckland, 1142,

17 New Zealand.

18 E-mail: ahmed.aljumaily@aut.ac.nz

19 Tel: (+649) 921 9777

20 Fax: (+649) 921 9973

1

2   **ABSTRACT**

3   Nasal morphology plays an important functional role in the maintenance of upper airway

4   health. Identification of functional regions, based on morphological attributes, assists in

5   correlating location to primary purpose. The effects of morphological variation on heat and

6   water mass transport in congested and patent nasal airways were investigated by examining

7   nasal cross-sectional MRI images from 8 healthy subjects. This research confirms the

8   previous identification of functional air-conditioning regions within the nose. The first is the

9   anterior region where the morphology prevents over-stressing of tissue heat and fluid supply

10   near the nares. The second is the mid region where low flow velocity favours olfaction and

11   particle deposition. The third is the posterior region which demonstrates an increase in heat

12   and water mass flux coefficients to compensate for rising air humidity and temperature.

13   Factors identified within the congested airway that favour enhanced mucocillary clearance

14   were also identified.

15

18

1.   INTRODUCTION

The mucociliary blanket in the nasal cavity provides the human airways with the first line of defence against infection, particles and airborne pollutants through entrapment in sticky mucus (Bossi et al., 2004; Cone, 2009; Widdicombe, 2002). Within the nose, this defensive layer is continuously transported towards the pharynx, where it is cleared by swallowing (Antunes et al., 2009) or expectoration. Mucocillary transport velocity (MTV) is significantly influenced by airway fluid hydration state (Button and Boucher, 2008) and normally ranges from 3-25 mm/min (Boek et al., 2002; Mygind and Dahl, 1998).

The interior nasal mucosa also provides heat and moisture to condition inhaled air and to prevent lower airway dryness (Doorly et al., 2008a; Rouadi et al., 1999). This air-conditioning function is achieved through the combined action of anatomical features, which include complex and narrow internal geometry (Croce et al., 2006; Doorly et al., 2008b; Segal et al., 2008; Wolf et al., 2004), and vascular/cellular regulatory systems (White et al., 2011).

1.1.   Nasal morphology

Modern imaging techniques, such as computed axial tomography (CT) and magnetic resonance imaging (MRI), have enabled the capture of accurate *in-vivo* nasal geometric information, which goes beyond that previously obtained by acoustic rhinometry (AR). Earlier investigations comparing CT and AR cross-sectional data has a good correlation within the relatively open anterior spaces of the nose (Çakmak et al., 2003; Hilberg et al., 1989). However, AR tends to underestimate cross-sectional area (CSA) beyond the complex and sometimes obstructed turbinate region (Cakmak et al., 2005). Post-processing of CT data

also provides additional morphological information unavailable through AR techniques, such as airway perimeter and total airway volume.

Previous analysis of flow trajectories has identified three functional regions within the two enantiomorphic parts of the nasal airways where nasal morphology is correlated to respiratory function (Mlynski et al., 2001):

1. The anterior tract, consisting of the vestibule, isthmus and anterior cavum, which act as a curved nozzle-diffuser that stabilizes and redirects airflow across the turbinates.

2. The mid functional tract, consisting of a slit-like space that presents a large mucosal surface area to the airflow.

3. The posterior tract, consisting of the posterior cavum, choanae and epipharynx, which act as a curved nozzle to stabilize and redirect airflow to the lower airways.

Many morphological studies have been undertaken to improve the functional understanding of geometry as well as the complex dynamic behaviour within this part of the human airway. These studies have resulted in many numerical models of heat and water mass transfer. Analysis techniques vary, but can involve direct importation of CT morphology data into computational fluid dynamics (CFD) software to provide airflow predictions within complex 3-D domains (Chen et al., 2010; Croce et al., 2006; Garcia et al., 2007; Lindemann et al., 2004; Pless et al., 2004). Other methods use mathematical models derived from continuity and transport equations, which are applied to simplified anatomic based geometry to predict airway heat and water mass transfer (Daviskas et al., 1990; Hanna and Scherer, 1986; Naftali, 1998; Tawhai, 2003; Tsu et al., 1988). In this case, the internal forced-convection coefficients for heat and water mass transfer are predicted by the non-dimensional Nusselt (N_u) and Sherwood (S_h) numbers, determined from two components:

1   1. Momentum to thermal diffusivity ratio to yield a Prandtl number (P_r) for heat transfer

2   or momentum to mass diffusivity to yield a Schmidt number (S_c) for mass transfer.

3   2. Airflow character, such as laminar or turbulent, predicted by Reynolds number (R_e)

4   (Cengel, 2006).

5 Under conditions of constant fluid properties P_r and S_c remain unchanged meaning airflow

6 character effectively governs the heat and water mass transfer coefficients. Airflow regime

7 state is normally identified by the magnitude of the Re, which expresses the ratio of inertia to

8 viscous forces as:

9 $$R_e = VD/\nu \qquad\qquad (1)$$

10 where V and D represent the mean fluid velocity and pipe diameter respectively, and ν

11 represents the fluid kinematic viscosity. When considering non-circular ducts, such as those

12 found within the nose, D is replaced with a hydraulic diameter (D_h) to account for interaction

13 between the moving fluid and boundary surfaces (Fox and McDonald, 1994; Sabersky et al.,

14 1999). This parameter describes the ratio of flow sectional properties, expressed

15 mathematically as:

16 $$D_h = 4 \text{xCSA/Perimeter} \qquad\qquad (2)$$

17

18 Through use of the continuity equation, air volume flow rate (Q) can be written as:

19 $$Q = V \text{ x CSA} \qquad\qquad (3)$$

20 In reality, the inhaled air physical properties do not significantly change during passage

21 through the nose. Given this, variation in CSA and D_h correspond to geometrical changes,

22 which directly influence the magnitude of R_e and hence the heat and water mass transport.

23

24 *1.2. Nasal Cycle*

1   It is well known that 20 – 40 % of the population (Davis and Eccles, 2004; Hanif et al., 2000)

2   experience periodic congestion/decongestion of the erectile tissue in each side of the nose

3   (Druce, 1988; Lindemann et al., 2003). This 'nasal cycle' results in alternating patent and

4   congested passages within the two enantiomorphic parts of the airway for periods ranging

5   from 1 – 7 hours (Kennedy et al., 1988). This time span is made up from combinations of

6   discrete ultradian periods spanning 1-1½ hours (Atanasov et al., 2003). The nasal cycle

7   usually goes unnoticed since the total nasal airflow resistance remains unaffected (Eccles,

8   1982; Wolf et al., 2004).

9

10   In this study, the nasal morphology of eight individuals was investigated using MRI

11   techniques. Unlike previous work, morphological analysis was used to identify functional

12   regions within the nose. To the best of our knowledge, no one has considered the distribution

13   of CSA and D_h throughout the two enantiomorphic parts of the nasal airway in terms of its

14   physiological significance to local heat and water flux. The difference in airflow between

15   patent and congested airways was also examined with regards to the nasal cycle.

16

17   **2.   MATERIALS AND METHODS**

18   *2.1.   Morphology acquisition*

19   Four male and four female healthy non-smoking participants, of mixed ethnicity and ages

20   ranging from 21 – 51 years and with no prior history of upper airway disease, volunteered for

21   the study. Ethical approval was granted by The Auckland University of Technology Ethics

22   Committee, application number 10/121, with each participant giving informed consent. Each

23   participant also undertook a visual nasal internal examination to ensure the absence of

24   morphological abnormalities such as significantly displaced septum, mucosal inflammation

25   or other nasal pathological conditions. All participants had not received any form of

1 medicine and had not consumed food for 2 hours, or alcohol for 24 hours, prior to

2 undertaking the MRI scan. They also undertook a maximal voluntary nasal ventilation test,

3 measured simultaneously from the nares, to determine the status of their nasal cycle

4 immediately prior to scanning. This test was repeated directly upon conclusion of scanning

5 to ascertain if changes in nasal cycle had occurred during testing. Participants were studied

6 in the supine position within a 3-Tesla MRI scanner (Siemens Magnetom Skyra) using a head

7 array coil. The region of interest within the nose spanned from the anterior isthmus to the

8 posterior choanae. Morphologic image acquisition used T1-weighted sagittal slices of

9 repetition time (TR) 700 ms, and echo time (TE) of 12.0 ms. Slice thickness was 0.78 mm,

10 echo spacing 4.05 ms and duration of each scan was approximately 5 minutes.

11

12 *2.2.   Airway measurement*

13 Post processing of acquired DICOM format MRI images was undertaken using 3 D-Doctor

14 ™ (Able Software Corp) to define airway boundaries using 0.78 mm coronal slices orientated

15 perpendicular to the floor of the nose. Nasal airway geometric properties for each participant

16 were compiled and plotted using MatLab ™ (MathWorks, Natick, MA, USA).

17

18 **3.   RESULTS**

19 *3.1   Geometry comparisons*

20 Figure 1 shows the distribution of morphological CSA and perimeter data along the nasal

21 airway vs. non-dimensional airway position (X/L), where X is the distance from the vestibule

22 and L is the total distance from the vestibule to posterior region of interest. Figure 1 presents

23 data for both patent and congested airways and demonstrates magnitudes and distribution

24 within the normal physiological range (Hilberg et al., 1989; Lang et al., 2003; Yokley, 2009).

25 Non-dimensional airway position is used to account for inter-participant variation in nasal

passage length.   The solid curve in each of these figures represents the line of best fit for

each parameter recorded and trends change in nasal morphology along the nasal passages.

The data in Figure 1 assumes uncorrelated residuals. While this is a questionable assumption,

and indeed a lag plot shows appreciable correlation between consecutive residuals, a formal

analysis using a Gaussian process (Hankin, 2005) shows that the effect of assuming

uncorrelated residuals is likely to be negligible. There is no information to support gender as

being a significant factor in the distribution of this data.

4.   DISCUSSION AND ANALYSIS

4.1   Cross sectional area distribution

Comparison of morphological properties between patent and congested airways (Figs. 1A to

1D) shows CSA as the only parameter that varies. The distribution of CSA (Figs. 1a & 1b)

correlates well with other data obtained by both AR and MRI techniques (Çakmak et al.,

2003; Cheng et al., 1996; Hilberg et al., 1989; Philip and Renato, 1996; Subramaniam et al.,

1998; Wen et al., 2008) and demonstrates the same variation occurring between patent and

congested airways (Lang et al., 2003). One participant demonstrated uncharacteristically low

CSA and perimeter results within their congested airway.

4.2.   Hydraulic diameter distribution

Figure 2 shows D_h vs. X/L and indicates that D_h in both human patent and congested airways

follows a similar trend; however, the former has relatively higher values than the latter. Both

of these compare poorly to patent and congested airways, measured using the AR techniques

(Lang et al., 2003), which ranged from 30-60 mm measured at the anterior head of the

inferior turbinate (not shown in Figure 2). Unlike imaging techniques used in this research,

rhinoresistometry measures flow and pressure in order to calculate D_h which may account for

1   this poor correlation. For comparison purposes, results previously obtained from human

2   cadaver mouldings (Hanna, 1983) are shown in Figure 2. These demonstrate slightly higher

3   values than the data obtained in this research which is probably due to unavoidable tissue

4   shrinkage and the absence of perfusion within cadaveric erectile tissue. D_h values measured

5   using MRI in live canine nasal airways (Craven et al., 2007) (also shown in Figure 2) over

6   the same region demonstrate similar results, both in terms of magnitude and distribution.

7   These close results may be attributed to both human and canine airways having similar

8   heating and humidifying functional requirements using similar tidal volumes.

9

10   *4.3.   Functional regions*

11   Examination of the D_h distribution along the non-dimensional airway (Figure 2) suggests the

12   presence of three distinct function regions (Mlynski et al., 2001). The first 20% (X/L=0.2) of

13   the anterior region of the airway is characterized by a reduction in which corresponds to a

14   progressive narrowing of CSA. The mid functional portion, covering a further 60% of the

15   airway is characterized by a constant minimum D_h value. Over this region, fluctuation in

16   CSA (Figs. 1 A & 1B) is counterbalanced by change in perimeter (Figs. 1 C & D). The

17   posterior portion, commencing approximately 80 % (X/L=0.8) into the airway, is

18   characterized by a rapid increase in D_h.

19

20   *4.4   Heat and water flux*

21   Assuming constant air physical properties identifies R_e as playing a major role in regulating

22   the heat and mass transfer processes within the nose. Figure 3A shows the distribution of R_e

23   vs. X/L. There is a significant reduction in R_e magnitude within the mid functional region of

24   both patent and congested airways. This indicates a reduction in flow velocity in this region

1   which favours olfaction function and particulate deposition as well as an increase in the

2   duration of time air is exposed to the mucosal surfaces.

3   Figure 3B shows the net heat and water flux (N-Flux$_{qw}$) vs. X/L. This variable, derived from

4   R$_e$ and airway surface area, effectively quantifies the total heat and water flux distribution

5   along the nasal airway. Cool and dry air potentially provides the greatest air-conditioning

6   challenges to the nasal mucosa by placing a disproportionate heat and water mass flux burden

7   on the anterior airway. To overcome this 'shock' effect, it appears that the initial anterior

8   region, covering the transition between the skin at the nares and middle airway epithelia

9   (X/L=0 – 0.20), has reduced N-Flux$_{qw}$. During tidal breathing, cyclic exchanges of heat and

10   water need to be distributed evenly along the mucosal surface to balance out tissue loadings.

11   A constant N-Flux$_{qw}$ value within the mid functional region of the patent airway must

12   contribute to achieving this under conditions of alternating airflow. This region covers the

13   majority of patent airway length (X/L=0.20 – 0.80) and results in progressive heating and

14   humidifying of inhaled air as it traverses the length of the nasal passage. Of note are the

15   fluctuating suppressed N-Flux$_{qw}$ values for congested airways. The posterior regions in both

16   patent and congested airways are characterised by an increase in N-Flux$_{qw}$ which would

17   ensure further heat and water flux occurs within this locale.

18   *4.5   Mucocillary clearance*

19   Periodic congestion/decongestion of the nasal airways has been shown previously to assist in

20   purging contaminants entrapped within the mucus layer of the congested airway (Soane et al.,

21   2001). In our investigation, reduction in N-Flux$_{qw}$ occurred at two locations within the mid

22   functional portion of the congested airway (Fig 3B). Although the purpose of the nasal cycle

23   is currently not fully understood, it is thought to play a role in balancing mucosal heat and

24   water fluxes (Elad et al., 2008), as well as allowing the cells on the congested side to rest and

25   recharge (Eccles, 1982). This reduction in N-Flux$_{qw}$ coincides with reduced air flow in the

1 congested airway and should result in no net change in air-conditioning of the combined

2 airways. Earlier research has found that the degree of water saturation did not correlate to

3 any position along the airway or time during the nasal cycle (Lindemann et al., 2003).

4 Reduced heat and water demand within the congested airway leads to replenishment of

5 airway fluid levels and additional mucus hydration, both of which have been shown to

6 improve MTV (Kilgour et al., 2004). Further, diminished airflow within the congested

7 airway also leads to a reduction in particulate and other airborne pollutant deposition rates

8 into the sticky mucus layer, further aiding mucocillary clearance. Since MTV is

9 predominantly regulated by purinergic mechanisms (Braiman et al., 2000; Bucheimer and

10 Linden, 2004; Button and Boucher, 2008), mucus transport acts independently of the nasal

11 cycle.

12

13 **CONCLUSIONS**

14 This investigation has identified three functional regions occurring within the nasal airways.

15 The anterior functional region of both patent and congested airways demonstrates a reduction

16 in N-Flux$_{qw}$ that prevents local stressing of underlying tissue heat and water supply. The mid

17 functional regions of the two enantiomorphic nasal airways demonstrate a reduction in R$_e$

18 which favours olfactory function and particulate deposition by increasing the time of air is

19 exposed to the mucosal surfaces. This functional region of the patent airway also experiences

20 constant N-Flux$_{qw}$ which balances tissue heat and water supply during the period of greatest

21 demand. The posterior region of both airways experience increases in N-Flux$_{qw}$ in order to

22 achieve further air-conditioning despite reduced driving gradients. Finally, reduced N-Flux$_{qw}$

23 occurs within the congested airway which supports earlier findings of enhanced mucus

24 clearance occurring within this passage.

25

1 REFERENCES

2 Antunes, M.B., Gudis, D.A., Cohen, N.A., 2009. Epithelium, Cilia, and Mucus: Their Importance in
3 Chronic Rhinosinusitis. Immunol. Allergy Clin. North Am. 29, 631-643.

4 Atanasov, A.I., Dimov, P.D., Dimitrov, B.D., 2003. Time periods in the nasal cycle during night sleep.
5 Biol. Rhythm. Res. 34, 355-366.

6 Boek, W.M., Graamans, K., Natzijl, H., van Rijk, P.P., Huizing, E.H., 2002. Nasal mucociliary transport:
7 new evidence for a key role of ciliary beat frequency. Laryngoscope 112, 570-573.

8 Bossi, R., Piatti, G., Roma, E., Ambrosetti, U., 2004. Effects of long-term nasal continuous positive
9 airway pressure therapy on morphology, function, and mucociliary clearance of nasal epithelium in
10 patients with obstructive sleep apnea syndrome. Laryngoscope 114, 1431-1434.

11 Braiman, A., Silberberg, S.D., Priel, Z., 2000. Purinergic stimulation of ciliary activity. Drug Dev. Res.
12 50, 550-554.

13 Bucheimer, R.E., Linden, J., 2004. Purinergic regulation of epithelial transport. J. Physiol. 555, 311-
14 321.

15 Button, B., Boucher, R.C., 2008. Role of mechanical stress in regulating airway surface hydration and
16 mucus clearance rates. Respir. Physiol. Neurobiol. 163, 189-201.

17 Cakmak, O., Çelik, H., Cankurtaran, M., Ozluoglu, L.N., 2005. Effects of Anatomical Variations of the
18 Nasal Cavity on Acoustic Rhinometry Measurements: A Model Study. Am. J. Rhinol. 19, 262.

19 Çakmak, Ö., Coşkun, M., Çelik, H., Büyüklü, F., Özlüoğlu, L.N., 2003. Value of Acoustic
20 Rhinometry for Measuring Nasal Valve Area. Laryngoscope 113, 295-302.

21 Cengel, Y.A., 2006. Heat and Mass Transfer: A Practical Approach, 3rd ed. McGraw-Hill, Singapore.

22 Chen, X.B., Lee, H.P., Chong, V.F.H., Wang, D.Y., 2010. Numerical simulation of the effects of inferior
23 turbinate surgery on nasal airway heating capacity. Am J Rhinol Allergy 24, 118.

24 Cheng, Y.S., Yeh, H.C., Guilmette, R.A., Simpson, S.Q., Cheng, K.H., Swift, D.L., 1996. Nasal Deposition
25 of Ultrafine Particles in Human Volunteers and Its Relationship to Airway Geometry. Aerosol Sci
26 Technol 25, 274 - 291.

27 Cone, R.A., 2009. Barrier properties of mucus. Adv. Drug Delivery. Rev. 61, 75-85.

28 Craven, B.A., Neuberger, T., Paterson, E.G., Webb, A.G., Josephson, E.M., Morrison, E.E., Settles,
29 G.S., 2007. Reconstruction and Morphometric Analysis of the Nasal Airway of the Dog (Canis
30 familiaris) and Implications Regarding Olfactory Airflow. Anat Rec (Hoboken) 290, 1325-1340.

31 Croce, C., Fodil, R., Durand, M., Sbirlea-Apiou, G., Caillibotte, G., Papon, G.F., Blondeau, J.R., Coste,
32 A., Isabey, D., Louis, B., 2006. In vitro experiments and numerical simulations of airflow in realistic
33 nasal airway geometry. Ann. Biomed. Eng. 34, 997-1007.

34 Davis, S.S., Eccles, R., 2004. Nasal congestion: mechanisms, measurement and medications. Core
35 information for the clinician. Clin. Otolaryngol. 29, 659-666.

36 Daviskas, E., Gonda, I., Anderson, S.D., 1990. Mathematical modeling of heat and water transport in
37 human respiratory tract. J. Appl. Physiol. 69, 362-372.

38 Doorly, D., Taylor, D.J., Franke, P., Schroter, R.C., 2008a. Experimental investigation of nasal airflow.
39 Proc. Inst. Mech. Eng. [H] 222, 439-453.

40 Doorly, D.J., Taylor, D.J., Schroter, R.C., 2008b. Mechanics of airflow in the human nasal airways.
41 Respiratory Physiology and Cell Neurobiology 163, 100-110.

42 Druce, H.M., 1988. Measurement of nasal mucosal blood flow. J. Allergy Clin. Immunol. 81, 505-508.

43 Eccles, R., (1982). Neurological and pharmacological considerations, in: Proctor, D.F., Andersen, I.
44 (Eds.), The nose: upper airway physiology and the atmospheric environment. Elsevier Biomedical
45 Press, Amsterdam, pp. 191-214.

46 Elad, D., Wolf, M., Keck, T., 2008. Air-conditioning in the human nasal cavity. Respir. Physiol.
47 Neurobiol. 163, 121-127.

48 Fox, W.R., McDonald, A.T., 1994. Introduction to Fluid Mechanics, 4th ed. John Wiley & Sons, New
49 York.

50 Garcia, G.J.M., Bailie, N., Martins, D.A., Kimbell, J.S., 2007. Atrophic rhinitis: a CFD study of air
51 conditioning in the nasal cavity. J. Appl. Physiol. 103, 1082-10925.

Hanif, J., Jawad, S.S.M., Eccles, R., 2000. The nasal cycle in health and disease. Clin. Otolaryngol. 25, 461-467.

Hankin, R.K.S., 2005. Introducing BACCO, an R Bundle for Bayesian Analysis of Computer Code Output. J Stat Softw 14, 1-21.

Hanna, L.M., (1983). Modelling of heat and water vapor transport in the human respiratory tract (air-conditioning). University of Pennsylvania, United States -- Pennsylvania.

Hanna, L.M., Scherer, P.W., 1986. Regional control of local airway heat and water vapor losses. J. Appl. Physiol. 61, 624-632.

Hilberg, O., Jackson, A.C., Swift, D.L., Pedersen, O.F., 1989. Acoustic rhinometry: evaluation of nasal cavity geometry by acoustic reflection. J. Appl. Physiol. 66, 295-303.

Kennedy, D.W., Zinreich, S.J., Kumar, A.J., Rosenbaum, A.E., Johns, M.E., 1988. Physiologic mucosal changes within the nose and ethmoid sinus: Imaging of the nasal cycle by MRI. Laryngoscope 98, 928-933.

Kilgour, E., Rankin, N., Ryan, S., Pack, R., 2004. Mucociliary function deteriorates in the clinical range of inspired air temperature and humidity. Intensive Care Med. 30, 1491-1494.

Lang, C., Grützenmacher, S., Mlynski, B., Plontke, S., Mlynski, G., 2003. Investigating the Nasal Cycle Using Endoscopy, Rhinoresistometry, and Acoustic Rhinometry. Laryngoscope 113, 284-289.

Lindemann, J., Keck, T., Wiesmiller, K., Sander, B., Brambs, H.J., Rettinger, G., Pless, D., 2004. A Numerical Simulation of Intranasal Air Temperature During Inspiration. Laryngoscope 114, 1037-1041.

Lindemann, J., Leiacker, R., Rettinger, G., Keck, T., 2003. The relationship between water vapour saturation of inhaled air and nasal patency. Eur. Respir. J. 21, 313-316.

Mlynski, G., Grutzenmacher, S., Plontke, S., Mlynski, B., 2001. Correlation of Nasal Morphology and Respiratory Function. Rhinology (Utrecht) 39, 197-201.

Mygind, N., Dahl, R., 1998. Anatomy, physiology and function of the nasal cavities in health and disease. Adv. Drug Delivery. Rev. 29, 3-12.

Naftali, S., Schroter, R.C., Shiner, R.J., Elad, D., 1998. Transport phenomena in the human nasal cavity: a computational model. Ann. Biomed. Eng. 26, 831-839.

Philip, C., Renato, R., 1996. The Nasal Valve and Current Technology. Am. J. Rhinol. 10, 23.

Pless, D., Keck, T., Wiesmiller, K., Rettinger, G., Aschoff, A.J., Fleiter, T.R., Lindemann, J., 2004. Numerical simulation of air temperature and airflow patterns in the human nose during expiration. Clin. Otolaryngol. 29, 642-647.

Rouadi, P., Baroody, F.M., Abbott, D., Naureckas, E., Solway, J., Naclerio, R.M., 1999. A technique to measure the ability of the human nose to warm and humidify air. J. Appl. Physiol. 87, 400-406.

Sabersky, R.H., Acosta, A.J., Hauptmann, E.G., Gates, E.M., 1999. Fluid Flow: A First Course in Fluid Mechanics, 4th ed. Prentice Hall, New York.

Segal, R., Kepler, G., Kimbell, J., 2008. Effects of Differences in Nasal Anatomy on Airflow Distribution: A Comparison of Four Individuals at Rest. Ann. Biomed. Eng. 36, 1870.

Soane, R.J., Carney, A.S., Jones, N.S., Frier, M., Perkins, A.C., Davis, S.S., Illum, L., 2001. The effect of the nasal cycle on mucociliary clearance. Clin Otolaryng Allied Sci 26, 9-15.

Subramaniam, R.P., Richardson, R.B., Morgan, K.T., Kimbell, J.S., Guilmette, R.A., 1998. Computational Fluid Dynamics Simulations of Inspiratory Airflow in the Human Nose and Nasopharynx. Inhal. Toxicol. 10, 91-120.

Tawhai, M.H., Hunter, P.J., 2003. Modeling Water Vapor and Heat Transfer in the normal and the Intubated Airways. Ann. Biomed. Eng. 32, 609-622.

Tsu, M.E., Babb, A.L., Ralph, D.D., Hlastala, M.P., 1988. Dynamics of Heat, Water and Soluable Gas Exchange in the Human Airways:1. A Model Study. Ann. Biomed. Eng. 16, 547-571.

Wen, J., Inthavong, K., Tu, J., Wang, S., 2008. Numerical simulations for detailed airflow dynamics in a human nasal cavity. Respir. Physiol. Neurobiol. 161, 125-135.

White, D.E., Al-Jumaily, A.M., Bartley, J., Somervell, A., 2011. Nasal Air-Conditioning During Breathing Therapy. Current Respiratory Medicine Reviews 7, 213-225.

1   Widdicombe, J.H., 2002. Regulation of the depth and composition of airway surface liquid. J. Anat.
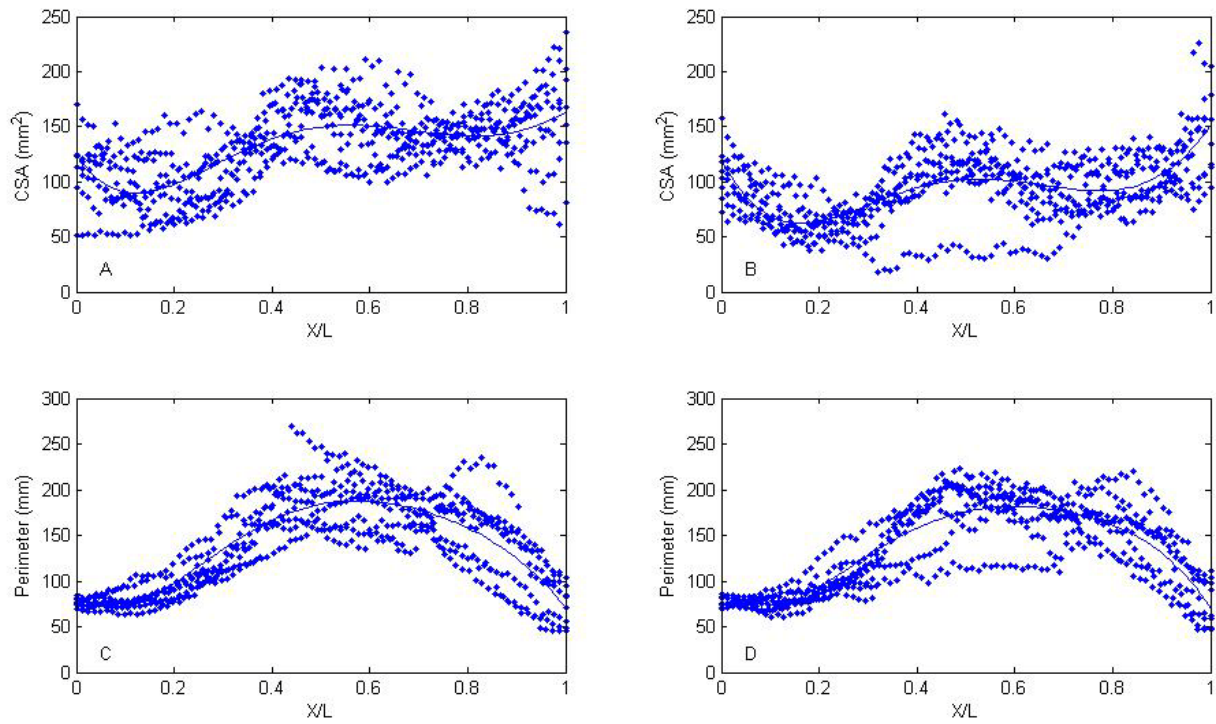2   201, 313-318.
3   Wolf, M., Naftali, S., Schroter, R.C., Elad, D., 2004. Air-conditioning characteristics of the human
4   nose. J. Laryngol. Otol. 118, 87-92.
5   Yokley, T.R., 2009. Ecogeographic variation in human nasal passages. Am. J. Phys. Anthropol. 138,
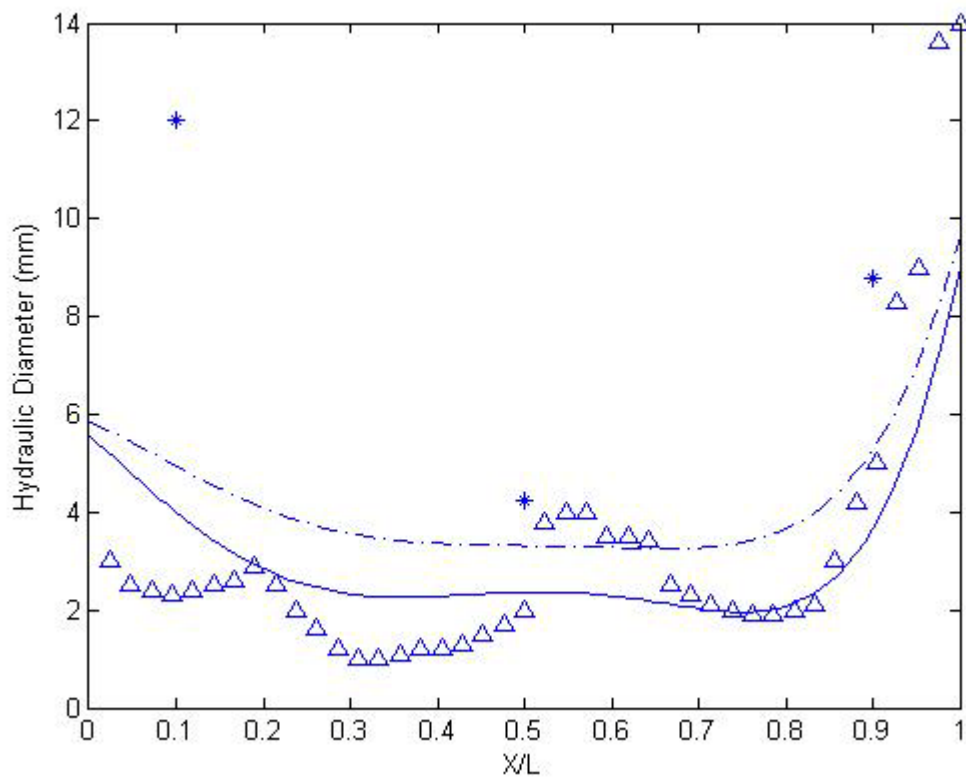6   11-22.
7
8

9

1

2   Figure 1: Distribution of participant morphological parameters. **(A)** Patent airway cross-

3   sectional area. **(B)** Congested airway cross-sectional area. **(C)** Patent airway perimeter. **(D)**
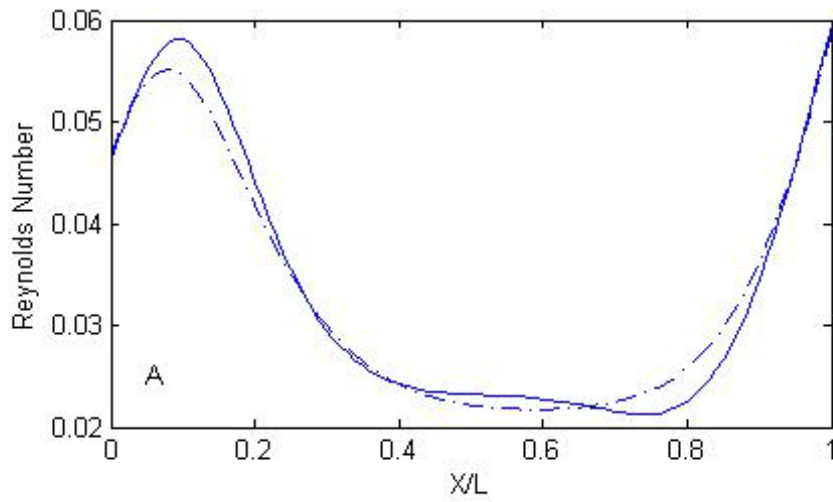
4   Congested airway perimeter.

5

1

2 Figure 2: Human and canine airway hydraulic diameter distribution: ─·─ human patent

3 airway (MRI), ─── human congested airway (MRI), △ canine airway (Craven et al. (2007),
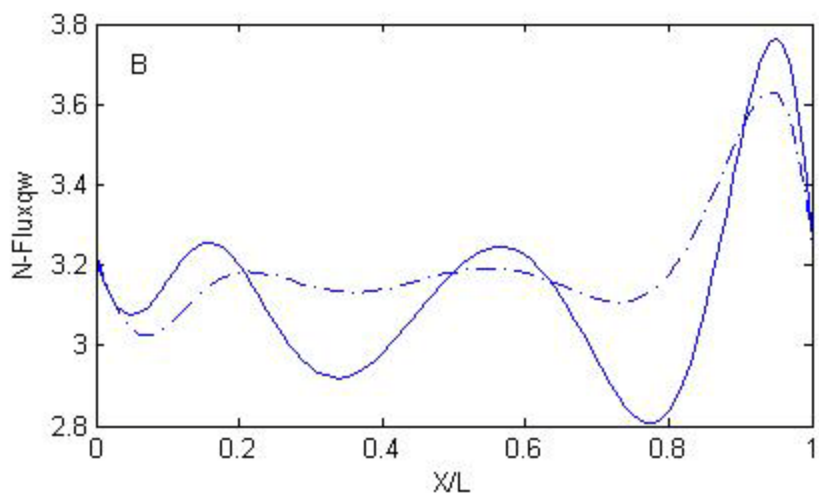
4 ∗ human cadaver (Hanna, 1983).

5

1

2

3

Figure 3: Distribution of airway heat and mass transfer components. (**A**) Reynolds number.

(**B**) Net heat and water flux coefficients. — · — human patent airway, ——— human congested

airway.

7

8

9